Proceedings of the ASME 2022 17th International Manufacturing Science and Engineering Conference
MSEC2022
June 27-July 1, 2022, West Lafayette, Indiana, USA

MSEC2022-85718

CURATING DATASETS OF FLEXIBLE ASSEMBLIES TO PREDICT SPRING-BACK BEHAVIOR FOR MACHINE LEARNING PURPOSES

Alex Adrian
The Ohio State University
Columbus, OH

Satchit Ramnath*
The Ohio State University
Columbus, OH

Sai Chandu Sunkara
Arizona State University
Tempe, AZ

Yannis Korkolis
The Ohio State University
Columbus, OH

Joseph K. Davidson
Arizona State University
Tempe, AZ

Jami J. Shah
The Ohio State University
Columbus, OH

ABSTRACT

There are many sources of manufacturing variations in sheet metal assemblies, such as automotive bodies. These include non-isotropic material properties from cold rolling, springback in stamping, and distortion from residual stresses when components are clamped and spot welded. FE simulations have been used to predict these variations in order to better design tooling and processes. Such simulations require expertise in complex, multi-stage nonlinear analysis. We are investigating the feasibility of training machine learning algorithms in order to democratize these types of analyses. This requires the curation of large, validated, and balanced data sets. To this end, we have developed a multi-stage finite element simulation workflow encompassing component stamping and joining with a focus on examining deformations due to springback in two-part assemblies. Three connected simulations comprise the workflow: (1) component stamping with capture of springback, (2) assembly clamping, and (3) assembly joining, then release. The workflow utilizes explicit dynamic finite element analysis (FEA) and includes the transfer of intermediate solutions (geometries/stresses), as well as extraction of key geometric parameters of springback from both component- and assembly-level simulations. The NUMISHEET 1993 U-draw/bending benchmark was referenced for its tooling geometry and utilized for verification of the forming process simulation; variations of material and geometry were also simulated. In summary, this work provides a means of generating a design space of flexible two-part assemblies for applications such as dataset generation, design optimization, and machine learning.

Keywords: data curation, sheet metal, springback, forming, stamping, joining, automated workflow, finite element analysis, dataset generation

1. INTRODUCTION

Mechanical products in general are assemblies made of multiple parts, either because of requirements for relative motion, use of different materials, or shape/size differences. Assembly design thus becomes the very crux of engineering design. Major design tasks typically include shape and size design of parts; interfacing of components; system layout and packaging; kinematic, dynamic, and structural analyses; and motion simulation and manufacturability analysis. In addition to the nominal geometry of an assembly, design also includes the assignment of tolerances to determine allowable manufacturing variations that ensure proper functioning and assemblability.

Large assemblies like the automotive body (Figure 1) are made up of flexible parts, such as sheet metal stampings. It is an assembly of many flexible subassemblies that are assembled and joined progressively. These subassemblies also are built progressively as shown in Figure 2. When two individually stamped parts are brought together to be joined into a subassembly, they often do not match up exactly, and so require special tooling and clamping to bring them into alignment. Thus, gaps between proximal assemblies must be precisely predicted and controlled. As subassemblies of parts are stacked, errors accumulate further. These tasks must be simulated in a holistic fashion because they involve the multiple disciplines of material science, structural design and analysis, forming mechanics, 3D tolerance analysis, and assembly design.

* Corresponding Author: ramnath.17@osu.edu

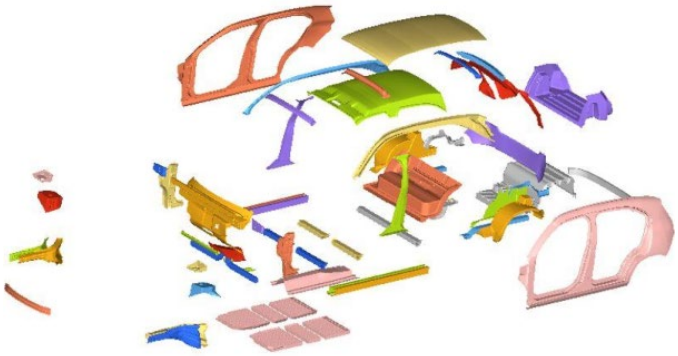

FIGURE 1: A COMPLEX FLEXIBLE ASSEMBLY [1]

Springback of a component is the geometric change it experiences at the end of the forming process when it has been released from the forces of the tool and die. Upon completion of plastic deformation from sheet metal forming, deep-drawn and stretch-drawn parts spring back elastically and distort the dimensional accuracy of a finished part. It is usually undesirable, causing problems such as increased geometric variability both for components in any subsequent forming operations and for assemblies made from the components. The use of AHSS (Advanced High Strength Steels), such as Dual Phase (DP), Mild Steel (MS) and Transformation Induced Plasticity (TRIP) grades in cold rolled form gives anisotropic properties and variable sheet thickness. The resulting complex or insufficient material models make the difficult problem of springback prediction even harder. As one example, automotive companies report having to re-machine dies multiple times to get the right shapes by trial and error [2].

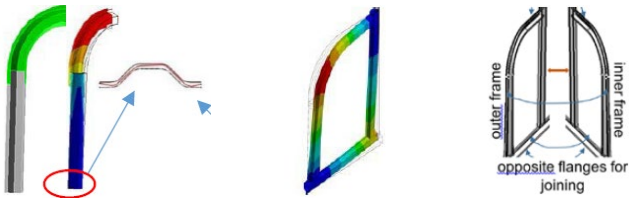

Simple Assembly | Closed Loop Assembly | Matched Pair Assembly

FIGURE 2: FLEXIBLE ASSEMBLY PROCESS

1.1 Research Goal

In the case of large assemblies, trial and error procedures used in practice today are costly and time consuming and cause delays in new product launch and quality problems. These drawbacks can be reduced or eliminated by using Artificial Neural Nets (ANN). When trained and validated, they offer the potential for data-driven rapid design space exploration. The upfront investment needed is in producing the required data by a combination of simulation and testing. In the long run, however, it pays off because design space is thoroughly explored, not only resulting in better designs but also facilitating future designs where some previously "rejected" designs may be pulled off the shelf for a new design. Our research proposes a method to curate large datasets, at various stages – from individual stamping to assembly, for training a set of ANN algorithms to work together to make predictions on the final outcome.

The datasets are curated using a multi-stage simulation workflow encompassing component stamping and component joining to form subassemblies/assemblies. Automotive body structures, such as the one shown in Figure 1, provide a real world application. These hollow structures are built from two matched (and opposite) hat section subassemblies joined at the flanges, which in turn are made by joining stamped hat-section components end-to-end (Figure 2).

2. BACKGROUND

With the rapid increase in computation power, finite element methods (FEM) for analyzing and predicting springback have become more attractive. Various benchmark tests [3][4][5] illustrate the state of the art in predicting springback with FEM. In particular, the 1993 benchmark [3] represents a flanged channel forming operation that was simulated using FEM, whose results were compared to experimental results.

In order to investigate the physical and numerical sensitivity of sheet springback simulations, draw-bend tests are analyzed using finite element modeling. The draw-bend test is chosen as a well-characterized example of a forming operation that produces springback similarly to industrial press forming operations. The test mimics closely the mechanics of deformation of sheet metal as it is drawn, stretched, bent, and straightened over a die radius entering a typical die cavity. As such, it represents a wide range of sheet forming operations, and has the advantage of simplicity [6].

2.1 Data Curation

For sales and business applications, large data sets are already available with companies like Amazon and Google. However, the volume and variety of data needed to train ANNs for specific engineering applications is limited like [7][8] generated using methods described in [9] and [10]; dataset specific to sheet metal stamping has to be curated and validated. That includes devising an integrated simulation pipeline for multi-stage process, and automating multi-stage simulation in order to produce large enough data sets for training. The flowchart (Figure 3) outlines the main aspects of the data generation pipeline. The output from each simulation not only feeds input to the next stage, but also extracts key parameters for use in the ANN pipeline.

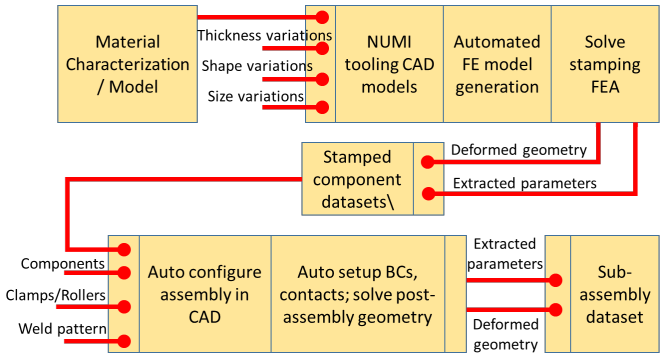

FIGURE 3: FLOWCHART FOR DATA GENERATION

Predicting variations in flexible assemblies is far too complex to be handled by a single ANN. Hence, it is necessary to curate data using abstractions, decompositions, and partitions of each data sample into sub-sets. This proposed research will provide insights into the data size, variety, balance and connectivity of spatial-geometric characteristics to design performance for engineering applications.

2.2 Current State of Art in Multi-stage Simulation

While every part is produced in multiple steps, including shearing, forming, joining and assembly, the current practice is to simulate each process independently, i.e., with little regard to the preceding steps and the effect these had on material properties, residual stresses, etc. Typically, only the geometry is transferred to the next step. Beyond simplification, this situation is driven by the lack of computationally efficient, robust, reliable and user-friendly material models that can handle non-proportional loading paths, multiple loading-unloading cycles, etc. Recently, it is being recognized that this occasionally leads to a break-down of the virtual process design cycle, i.e., the predictions do not match the experiments, parts fail in practice but not in simulation or vice-versa, etc. A notable example is the effect of a sheared hole/edge on the formability in subsequent stamping operations; while it is clear that using the formability of the as-received sheet leads to erroneous predictions of stamping (i.e., part failures that cannot be predicted), there still hasn't emerged an efficient and robust way of including the effect of the previous shearing in forming simulations.

One of earliest work was that of Hu [11] who modeled parts as linear springs in series or parallel, which is only applicable to simple 1D stacks. A more elaborate treatment is Hu [12] where linear FEA is used to determine key point deformations. In order to reduce the number of variables, they classified surface "deformation patterns" into a small number of typical patterns seen in manufacturing (convex, concave, single wave), and used Principal Component Analysis (PCA) to extract those patterns from "simulated" measurements of individual components in their free state.

The approach used in Merkley, *et al.* [13] bears similarities to both of the above. They also model components as linear springs in parallel or series but obtain the stiffness values from 2D FEA. However, the objective appears to be the calculation of six-sigma range of residual stresses in order to keep them below allowable max stress. Further evolution of this approach was done by Bihlmaier [14] and Mortensen [15]. The former used spectral analysis to extract deformation patterns to reduce model size. Instead of Monte Carlo simulation, using equations based on surface deflection dependencies (material covariance, in plane, and geometric covariance, out of plane). Mortensen used rigid body tolerance analysis to find mean and variance of gaps at weld locations, FEA to determine loads and stresses in closing the gaps and covariance analysis as above to reduce model size and perform statistical analysis. Model setup requires many manual steps and there is no relation to ASME Y14.5 [16] tolerance classes and tolerance zones.

Soderberg [17] defined a robustness metric for evaluating flexible assembly fixturing schemes (number and locations of clamps) based on sensitivity to deflections due to small variations in clamp location. Starting with a 3-2-1 clamping, a user can introduce multiple clamp locations and evaluate plots of the robustness metric. In further application of this approach, Forslund [18] uses genetic algorithms (GA) to optimize the fixturing scheme for each assembly based on its specific misalignments.

Our approach is far superior to prior work on flexible assemblies that have used over simplified structural stiffness models to determine the effects of tooling misalignments and residual stresses due to clamping (Hu [11][12], Ceglarek [19]). The studies that did use FEA (Merkely [13], Bihlmaier [14] and Mortensen [15]) are not applicable to generating large data sets for machine learning because many manual steps are needed and there is no relation to Y14.5 standard tolerance classes and zones. Others have used optimization methods to determine best fixturing locations for specific assemblies, (Forslund [18], Moos [20]). Hashemian et al [21] considered the last assembly step in attaching automobile roofs welded to a rigid frame. They compared coordinate-measuring machine (CMM) data to Monte Carlo models of curvature variations of the roof. In recent years commercial GDT) tools, such as 3DCS and VisVSA, have incorporated FEA for flexible assembly variability analysis. However, because there is little integration of these models, results are not reliable.

From these reviews, we can conclude that predicting variability in flexible assemblies, such as automotive body structures, remains an unsolved problem, despite the economic benefits it can yield for industry. Studies so far are limited both in several ways: in their scope, (to one or two stages in the process chain); in the range of variables considered (material, tooling, work piece, dimensional and geometric parameters); and over-simplified shapes. The diverse slices in dealing with each of these aspects cannot be integrated because of incompatible models and impractical scalability. A holistic approach is needed that considers the entire pipeline, from AHSS anisotropy to

component variability to multi stage assembly and joining variability. Traditional approaches to solving this problem, such as DOE cannot handle the number of variables. Therefore, we turn to the non-traditional approach of a network of ANNs.

3. SIMULATION WORKFLOW

To generate the volume of data needed for this investigation, a multi-stage explicit finite element simulation workflow has been developed. In addition to the simulation workflow itself, methods for extracting, processing, and curating key results from the simulations have been applied. The following sections outline the overall scope of the workflow, the verification of the forming simulation using existing benchmarks [3][22], the organization and modeling procedure of each simulation in the workflow, and the extraction, processing, and curation of the results.

3.1 Scope of Workflow

The simulation workflow consists of three separate but dependent explicit finite element analysis stages. At a high level, the workflow simulates the forming of individual hat section components and the joining of sets of two components at a time, as demonstrated in Figure 4 for a single assembly case.

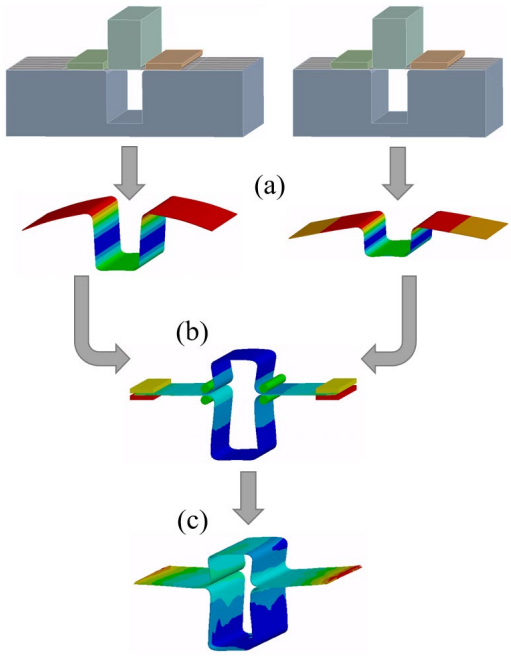

FIGURE 4: OVERVIEW OF SIMULATION WORKFLOW

The first analysis stage (Figure 4(a)) simulates the forming and springback of hat section components from blank sheets, leveraging the NUMISHEET 1993 2D U-draw/bending benchmark [3] for its tooling geometry and forming process, as well as the material properties used in a separate investigation [22] based on the same benchmark. At this stage, variations of tooling geometry, process parameters, and material are used to generate more diverse components for inclusion in additional assemblies.

The second analysis stage (Figure 4(b)) involves selecting two compatible components and clamping them together in preparation for spot welding. Since this stage requires inputs from two separate forming simulations, deformed meshes and associated stresses/strains are imported from the previous stage and transformed into the clamping arrangement shown in Figure 4. At this stage, the specific hat sections selected for joining are varied while ensuring compatibility to generate multiple assembly configurations.

The third analysis stage (Figure 4(c)) includes addition of simplified spot welds between the flanges of each component, followed by release of the clamps. This allows the assembly to deform based on residual stresses carried over from forming and clamping. As such, deformed meshes and associated stresses/strains must be imported from the previous stage here as well.

Results of engineering significance are extracted after the forming and joining stages. Extracted results generally consist of deformations along pre-defined sections and edges; these results are then processed into parameters describing post-forming springback and post-joining twist. These results, as well as key input parameters, are curated into a dataset which maintains relationships between the input and output parameters of the workflow. In this way, the dataset is organized such that future training of developed ANNs can be performed efficiently. In addition, the workflow's parameterization allows for future automation, which could result in generation of even larger datasets in relatively short amounts of time compared to running each simulation manually.

3.2 Forming Simulation Validation

To gain confidence in the forming-stage simulations, the process was first validated against an existing set of experimental and simulated results [22] based on the NUMISHEET 1993 benchmark [3]. For this validation study, a 1.2mm-thick 350mm x 45mm sheet of DP590 AHSS was formed in an explicit finite element analysis using Ansys LS-DYNA. The specific material properties used in the simulation were derived from those calculated in uniaxial tension and U-draw/bending tests [22]; these are summarized in Table 1. The elastic-plastic material model (Figure 5) utilizes isotropic elasticity and multilinear isotropic hardening. Since the forming process is quasi-static and inertial loads are not significant, the density of a generic structural steel material was used. The tooling geometry used in the simulation follows the benchmark [3] and is shown in Figure 6. While this validation was used to gain confidence in the first stage of the workflow, it was performed outside of the workflow and would not be transferred to any additional downstream simulation. Therefore, only a quarter of the total model was needed due to symmetry in the geometry, material, and loading. LS-DYNA Type 10 linear

quadrilateral shell elements (2mm x 2mm) with 5 through-thickness integration points were used for the blank sheet, while rigid solids were used for the punch, blank holder, and die. Stiffness-based hourglass controls (LS-DYNA Type 4, magnitude 0.05) were applied to the sheet as well. The punch was lowered to its maximum depth of 70mm at a constant speed of 100mm/s, held there for 0.025s, and then was raised at a constant speed of 190.5mm/s in real time, resulting in a simulated end time of 1.25 seconds. The simulated force applied to the blank holder was 6.4kN (one-quarter of the actual 25.7kN) from 0s – 0.8s and general frictional contact with a coefficient of 0.14 was applied between the sheet and all solid bodies.

Table 1. Material Properties for Simulated DP590 Steel

Density [kg/ mm^3]	E [GPa]	Poisson's Ratio	Yield Strength [MPa]
7.85E-06	191	0.30	411

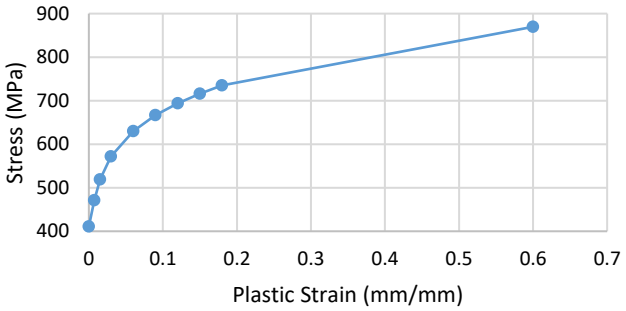

FIGURE 5: MULTILINEAR ISOTROPIC HARDENING CURVE

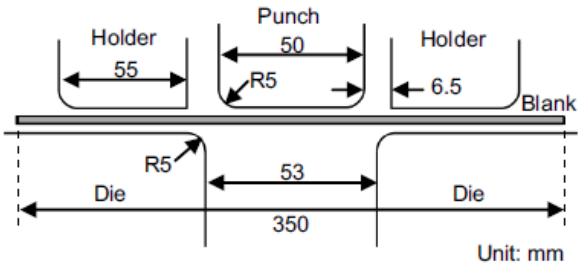

FIGURE 6: BENCHMARK GEOMETRY [22]

The deformed shape was extracted and plotted in the same manner as in [22] for direct comparison; the simulated and reference plots are shown in Figures 7 and 8, respectively. As shown, the deformed shape and amount of springback resulting from the validation simulation are both generally close to those seen in [22], building up confidence in the finite element model to be used in the first stage of the simulation workflow.

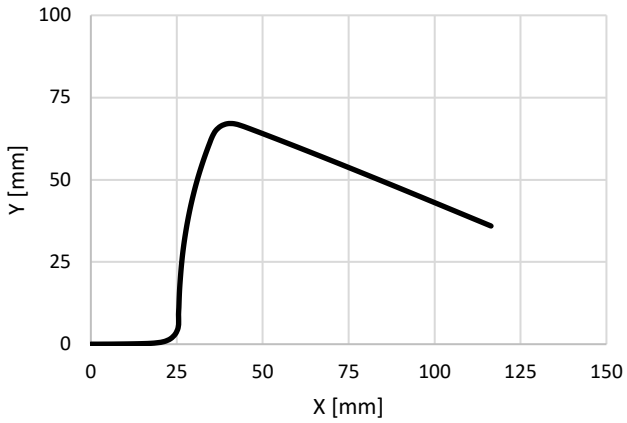

FIGURE 7: DEFORMED SHAPE FROM SIMULATION

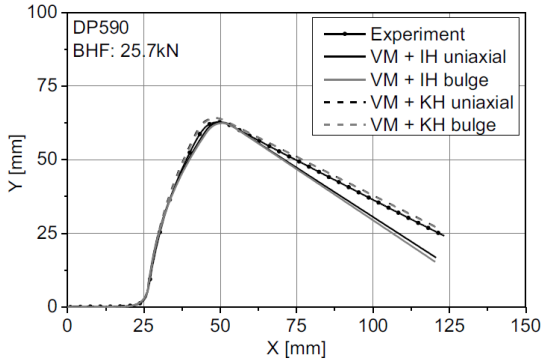

FIGURE 8: DEFORMED SHAPE FROM REFERENCE [22]

3.3 Forming Simulation – Workflow Stage 1

The FE model used for the component forming stage of the simulation workflow follows largely the same organization as the validation study, with the most apparent difference being simulation of the full 3D geometry for a hat section length of 305mm (12in) without the model reduction via symmetry, as the deformed geometries and residual stresses must be incorporated as inputs to downstream clamping simulations. The material model, tooling geometry profile, element types, contact interactions, and hourglass controls were all identical. In addition, symmetry boundary conditions applied at the blank sheet's centerlines were carried over, as the process is still theoretically symmetric. However, due to the long solution time of the validation study simulation being too high to allow for efficient future automation of the workflow (4 hours for a thin quarter-symmetric model), additional changes were made to allow for more reasonable solution times without the need for greater computing power. While this ultimately causes less springback to be exhibited in formed components, it does not prevent achievement of the overarching goals in this investigation: generating a curated dataset of flexible assembly data for applications in future ANN training.

These changes to the forming simulation model are a larger element size (3.125mm x 4.5mm), a shorter process time of 0.125s, and the introduction of automatic mass scaling to meet a time step size of 3E-06s. In this modified simulation, the punch travels 70mm down in 0.06s, holds position for 0.01s, raises 70mm to its original position in 0.0175s, then raises another 30mm above its original position in 0.0125s. The next 0.025s in the process does not involve any punch travel, but allows additional time for the springback of the formed hat section to occur. After making these modifications, the solution time for a full-sized component of the same draw depth as the benchmark [3] becomes 50 minutes. For additional components of different depths, the times for each step are adjusted to match the punch travel speeds and leave equal time for springback after punch removal.

The most significant difference between the simulated deformed components and those from [22] is a reduced curvature in the sidewall due to springback, as shown in Figure 9. A likely source of this variation is the element size used in each simulation and the use of linear elements. In the simulation of [22], 1x1.5mm sized elements were used, whereas the 4-hour and 40-minute simulations used sizes of 2x2mm and 3.125x4.5mm, respectively. The use of linear elements also reduces the effect of the bending/unbending over the die radius during the forming simulation, an effect which increases with element size.

The final springback parameters for the 4-hour and 40-minute simulations are summarized below in Table 2. These are the same parameters used later in section 4.1.

Table 2. Examples of Variety in Forming Simulation Stage

Profile	θ_1, deg	θ_2, deg	ρ, mm
4-hour Sim	104.5	77.59	142.8
40-min Sim	93.12	78.22	497.6

Several iterations of element size were tested to ensure acceptable mesh convergence. As element size decreased, specifically below 3.25mm, results became close to the profiles shown in the results of [22], exhibited by Figure 9. When element sizes larger than 3.5mm were used, almost no springback occurred and in some cases with element sizes larger than 4mm, springback appeared to reverse direction. For this reason, the size of 3.125mm used in the 40-minute simulation became the ideal choice for minimizing solution time while also producing enough springback. All the simulations were run on a 4-core machine with 2.8 GHz CPU and 32 GB RAM.

Key outputs from this simulation stage include deformations at multiple profiles along the length of the component (front, center, back), the deformed mesh of the component, and residual stresses/strains associated with the mesh. The profile deformations are extracted and processed for calculation of multiple parameters describing the springback as defined in the benchmark [3], which will be discussed with more detail in Sections 3.7, 4.1, and 4.2. Using the center profile deformation, a similar plot of the deformed shape is shown in Figure 9 for comparison to Figures 7 and 8 for reference of the results after process modification.

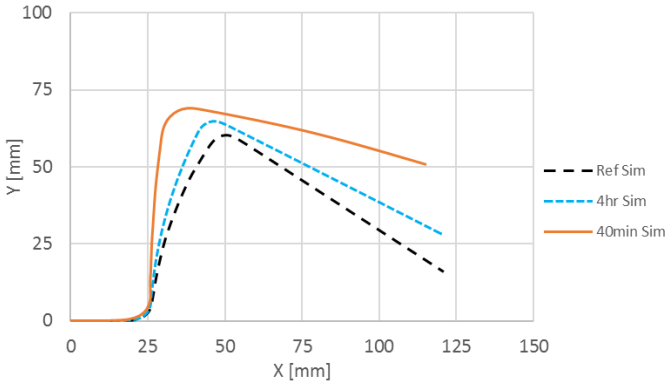

FIGURE 9: COMPARISON OF DEFORMED SHAPES FROM REFERENCE, 4HR AND 40MIN FORMING SIMULATIONS, REPRESENTED AS SETS OF SPRUNGBACK POINTS.

In addition to modifications being made to the process being simulated, additional variations of both geometry and material have been considered in the workflow for generating additional variety in the dataset. Geometric variations include additional nominal shapes (i.e. straight, curved, tapered hat sections), sheet thicknesses, and hat section depths, as well as changes to the geometric parameters of the tooling, while material variations include modifications to the nominal material (i.e. AHSS, aluminum alloy) as well as adjustments to the stress-strain curve, which is input to the simulation as the elastic modulus and a table of values for the plastic strain region. For a few specific examples of these variations (which are a subset of what is possible to generate using this workflow), refer to Table 2. Note that Table 3 shows a hat section depth of 0mm for one instance; this indicates a flat sheet, which would not require a forming simulation (only a mesh) but is included in the variations of components generated for assembly in the succeeding workflow stages.

Table 3. Examples of Variety in Forming Simulation Stage

Hat Section Shape	Material	Thickness [mm]	Depth [mm]
Straight	DP590	1.2	70
Straight	DP590	1.2	35
Straight	DP590	1.2	0
Straight	DP590 +20% stress in plastic region	1.2	70

3.4 Component Selection and Intermediate Solution Transfer

Following the component-forming stage of the simulation workflow, pairs of components must be selected for assembly and their intermediate solutions (deformed mesh with residual stresses/strains) must be transferred to the downstream

simulation stages. Criteria for assembly compatibility consists only of suitable geometric similarity, including hat section channel width, flange width, and overall length (including a flat sheet sized to match the channel + flange width and overall length). Differences in draw depth, thickness, and material between the selected components are desirable to create additional variability in the dataset of assembled components. As such, any combination of the component variations listed in Table 2 would be possible for assembly, assuming all come from the same tooling geometry.

Once selected for assembly, each component's deformed mesh (including local shell thicknesses) and residual stresses/strains are imported to an intermediate FE model, in which they are transformed to their proper assembly orientation ahead of the clamping simulation stage of the workflow. The intermediate model allows for component transformations (translation + rotation) while maintaining associativity between the mesh and the residual results. Within the Ansys Workbench software package, this was implemented using an external model system for each component and an imported .k file which was generated at the end time of each component's forming simulation.

At the end time of the clamping simulation (to be discussed in the next section), the same type of file is output such that this process may be repeated for importing clamping results into the joining simulation. In this intermediate stage, however, only one intermediate FE model is needed and no transformations are required. Another difference here is that the clamps themselves, in addition to the clamped sheets, are transferred to the joining stage. The specific reasons for this will be explained in the following sections.

3.5 Clamping Simulation – Workflow Stage 2

After two specific components are selected for joining, the flanges must first be clamped together to ensure contact where the simplified spot welds are to be located before the simplified spot welds may actually be added. In this workflow, the clamping occurs in its own simulation stage, separate from the joining/release, due to the specific modeling procedure used in adding the spot welds; this will be discussed in detail in the next section. The clamping simulation for each assembly configuration requires inputs from three different intermediate FE models: two component models, as discussed in the previous section, and a model containing clamps and guide rollers as meshed solids. The same clamp FE model is imported into all clamping simulations of a given component length, as the solid bodies can be transformed to prevent initial penetrations post-import, which significantly decreases the complexity of including this model as an additional input. An overall mesh imported from two forming simulations and the clamp FE model is all shown in Figure 10. Note that while two hat sections are shown here, this same process applies to assemblies containing flat sheets as well.

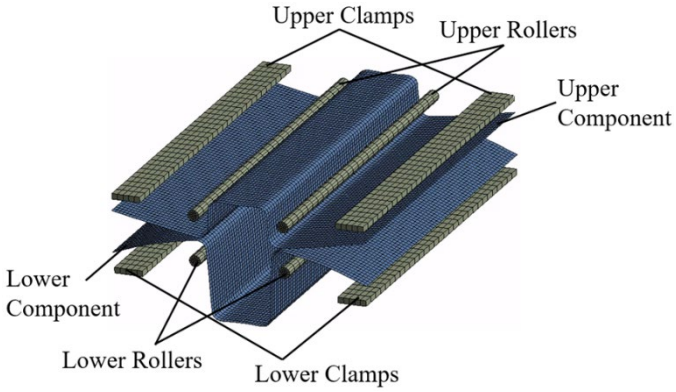

FIGURE 10: EXAMPLE OF MESH IMPORTED INTO CLAMPING SIMULATIONS

The clamps and guide rollers work together to ensure as much of the flange is in contact at the end time of the clamping simulation as possible. Whereas the solids used in the forming stage simulation are modeled as rigid bodies, those used for the clamps and guide rollers in this stage are modeled as flexible solid bodies. In this way, they are included in the mesh that is transferred to the joining simulation. While the components retain the same material model and mesh as were used in their respective forming simulations, the clamps and guide rollers must be modeled independently in their separate FE model before being imported. The cross-sectional shapes of the clamps and rollers are 5mm x 25mm rectangles and 10mm-diameter circles, respectively, and their length is equal to that of the hat sections. The material model used for these solid bodies is purely linear isotropic elasticity with a density of 9.0 e^{-6} kg/mm^3, modulus of elasticity of 1000GPa and a poisson's ratio of 0.3. The logic behind the values used was to take a generic structural steel and increase its density and stiffness to the point where the clamps and guide rollers would be approximately rigid compared to the formed components. The solids were meshed using LS-DYNA Type 1 linear hexahedral solid elements with a length of 10mm in the channel direction. In the width/height directions, a size of 5mm was used for the clamps and 2.5mm for the guide rollers, which were chosen for being the largest sizes to accurately represent the solids' cross-sectional geometry.

Between the sheets themselves, as well as the sheets and each solid, frictional contact with a coefficient of 0.10 was used. This value was determined to generate enough friction to hold the sheets firmly in place without inducing additional tangential contact stresses in the sheets. The clamps and guide rollers start outside of initial contact with either component and are displaced to be the exact distance of two sheet thicknesses apart over a 0.02s time interval, followed by 0.0175s of settling time to yield a simulated end time of 0.0375s. No additional boundary conditions are applied to the model, meaning all deformation in the sheets is a result of their contact interactions with the solids and each other. This has been shown to take about 10 minutes to solve, depending on the exact assembly configuration. At the

simulation end time, another *.k file containing the entire mesh shown in Figure 10 along with associated residual stresses/strains is exported for use in the joining simulation.

3.6 Joining Simulation – Workflow Stage 3

The joining simulation is the final stage of the simulation workflow and involves importing the mesh output from the clamping stage, creation of simplified spot welds between two clamped sheets, and release of the clamps and guide rollers. This allows for assembly-level deformations resulting from the built-up residual stresses in each component. The joining stage is separate from the clamping stage due to the method of modeling the simplified spot welds, which will be discussed here. All previous model settings for the two components and the clamps/guide rollers are carried over from previous workflow stages, so creation of the spot welds is the most significant modeling required at this workflow stage.

Before spot welds are actually modeled, their locations must be decided, which gives rise to an additional opportunity for variation in the dataset generated by this workflow. So far, however, the weld pattern has been held constant: three welds along the length of each flange with one centered along the length and the others spread apart from the center evenly, distanced 25.4mm (1in) from each end, as shown in Figure 11(a). At these locations, body-to-body beam connectors are inserted between the two sheets to simulate the presence of weld material. The beam connectors themselves are 3mm-diameter cylinders with the same approximately rigid material as the clamps and rollers, detailed in the previous section. Each end of each beam connector is coupled in all degrees of freedom (Ux, Uy, Uz, Rx, Ry, Rz) to the nodes falling within a 5.5mm radius of the weld location on the respective sheet, which is similar to the size of an automotive body spot weld and large enough that stresses may be transmitted through the beam connectors without high concentrations on either sheet. Figure 11(b) shows close-up images of these beam connectors and their couplings with nearby nodes. With this methodology, the simplified spot welds are essentially rigid connections between sets of nodes on either sheet. This type of connection cannot be generated during a simulation and must be created between geometry which is already in place at the simulation's initial time, which explains the division of the clamping and joining stages of the workflow. Figure 11 shows an overall assembly mesh after being imported from the clamping stage and connected with the simplified spot welds.

In addition to creation of the spot weld surrogate models, contact between the bodies is defined in the same manner as was done for the clamping simulations. The load steps of this simulation stage involve displacement of the clamps and guide rollers until they are far out of contact with either sheet over the first 0.01s, followed by 0.025s of settling time to allow the assembly to deform due to the residual stresses. The only support included in the model is a fixed node in the center of the bottom component to prevent rigid body motion after removal of the clamps and guide.

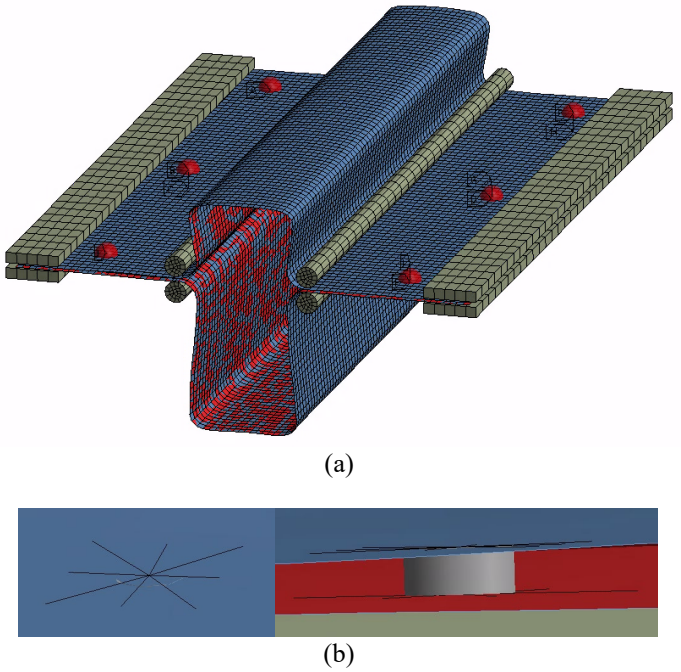

(a)

(b)

FIGURE 11: EXAMPLE OF INITIAL MESH AT JOINING STAGE SHOWING (a) LOCATIONS AND (b) CONNECTIONS OF SIMPLIFIED SPOT WELDS

This simulation stage has been shown to reach a solution in about 8 minutes, depending on the specific assembly configuration. Since there are currently no additional simulation stages in the workflow following the joining stage, the assembly-level results are ready for extraction, processing, and curation after this stage is solved.

3.7 Results Extraction, Processing, and Curation

As mentioned previously, key results of engineering significance are generated from the deformed geometries following both the forming simulation stage and the joining simulation stage. In this section, the exact methods of extracting data from FE solutions, processing them into results, and curating these results based on input parameters will be discussed in greater detail.

Before results may be extracted from the finite element simulation stages, solutions within each model must be organized. In both the forming and joining simulation stages, key FE results for extraction include deformations along pre-defined paths within each model. Examples of these path definitions are shown in Figure 12. For each path – defined prior to simulation execution, deformations in each direction are generated, which may then be extracted into spreadsheets, allowing for calculation of the final positions of each node along the respective path.

These final positions may then be processed into the results set for the overall dataset generated by this workflow.

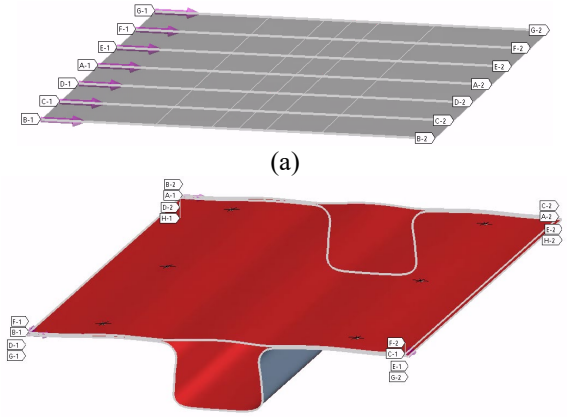

(a)

(b)

FIGURE 12: EXAMPLES OF PATHS DEFINED FOR FE RESULT EXTRACTION FROM A (a) COMPONENT AND (b) ASSEMBLY

With the FE simulation output data processed into key results (examples in Sections 4.1 and 4.2), the inputs and outputs to the workflow must be curated into a dataset in such a way that it can be leveraged in training of future ANNs. For this dataset, the curation and organization method involves formulation of a theoretical multi-dimensional matrix, with there being as many dimensions as input parameters to the workflow. Each dimension is represented by a specific input parameter such that a series of inputs (magnitudes in each dimension of the matrix) will yield a unique set of output results (assembly-level twist with corresponding component-level springback). The physical structure of such a matrix could take the form of a set of nested folders (wide accessibility) or an indexed data structure within a specific program (limited accessibility) that an ANN algorithm can be trained to scan through during training. This curation is part of the ongoing work to apply the dataset generated from the described workflow to yield engineering design outcomes.

4. RESULTS AND DISCUSSION

As mentioned previously, the key results generated by this workflow come from the component forming stage and the assembly joining stage. Using the previously outlined methods for results' generation, extraction, and processing, a dataset has been prepared for curation and use in training of ANN algorithms. In this section, a subset of this dataset is shown for reference of the types of results generated by the workflow and available for curation.

4.1 Component-Level Results

In this section, a subset of the results available at the component level is shown. Figure 13 shows the deformed geometry with a contour plot of residual stresses for a straight, 1.2mm thick, 35mm deep DP590 hat section generated from the NUMISHEET tooling [22]. Figure 14 exhibits directional deformations available along a single path in the same component, which becomes an exported result for additional processing into springback parameters.

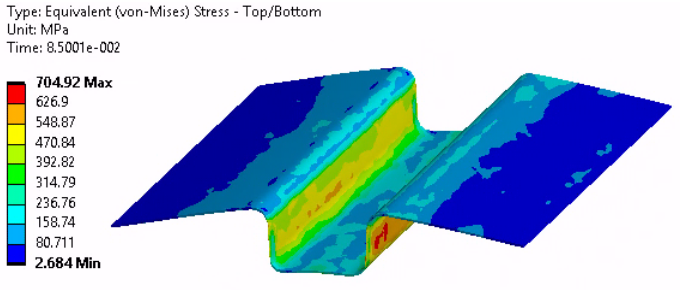

FIGURE 13: EXAMPLE OF DEFORMED GEOMETRY AND RESIDUAL STRESSES IN A FORMED COMPONENT

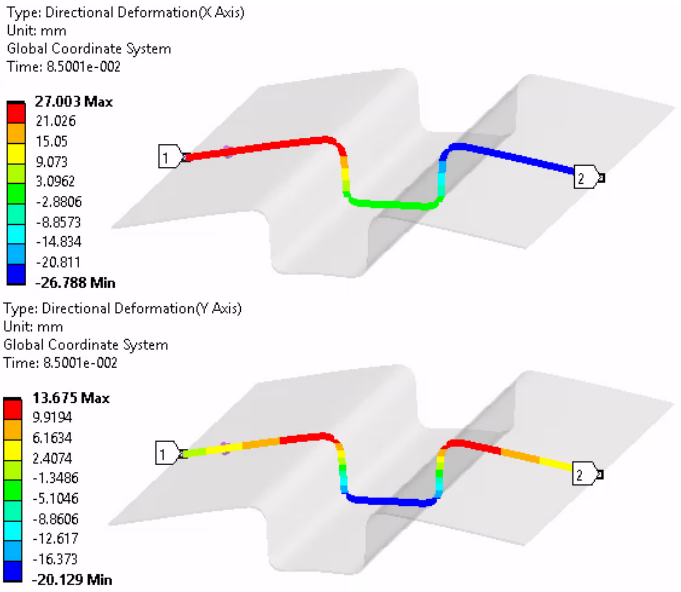

FIGURE 14: EXAMPLES OF DIRECTIONAL DEFORMATIONS ALONG A SINGLE PATH IN A FORMED COMPONENT

The three NUMISHEET '93 parameters identified in [3] are the angles θ_1, θ_2, and arc-radius ρ, as shown in Figure 15. Angle θ_1 is measured between the x-axis and line AB, θ_2 between lines AB and EF, and ρ from the arc defined by points A and B and a mid-point C. In digitizing the computation of several parameters, a defined line or arc intersects the set of springback points (e.g. Figure 9) along the *interior* of a line-segment defined by two adjacent points of the set. If this interior condition is not met, another nearby pair of adjacent points is chosen. Point A comes from the intersection of a line 15 mm above the x-axis, point B as the intersection with the arc of radius 35 mm from A, and C as the intersection with the perpendicular bisector of AB. The radius ρ is computed from points A, B, and C with the algorithm in the Appendix of [23].

When the element size is small, the point-set shown in Figure 9 is more dense, and a reversed curvature with a slight downward bulge can be detected between points *D* and *E* (Figure 15). Point *D* at the end of the die-radius may then be found digitally as the peak of this bulge by computing distances to the local point-set from a line constructed parallel to a tentative line *EF*. However, when larger elements are used, as in this study (§3.3), the bulge is not detectible, but the highest sprungback node on the 5 mm radius is. Therefore, for this study, we ignore point *D* and instead find point *E* directly. It is found consistently as the intersection of a 15 mm arc, centered at the highest node on the 5 mm arc above *B*, with the *interior* of a line-segment defined by two adjacent points of the set further to the right (Figure 15). Point *F* is found similarly with an arc centered at *E* and of 40 mm radius.

The three NUMISHEET '93 parameters are shown in Table 4 for three cross-sectional profiles along the length of one component: those at the front, the center, and the back.

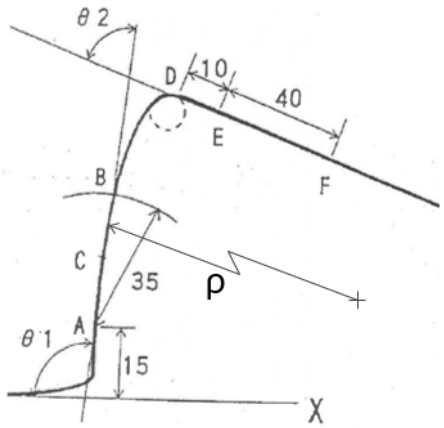

FIGURE 15: NUMISHEET '93 PARAMETERS θ_1, θ_2 AND RADIUS OF CURVATURE (ρ) FOR ARC ACB AS DEFINED IN [3].

Table 4: Examples of Calculated Springback Parameters from a Full-Depth Formed Component

Profile	θ_1, deg	θ_2, deg	ρ, mm
Front	92.98	78.38	782.9
Center	93.12	78.22	497.6
Back	93.16	78.47	9016.0

4.2 Assembly-Level Results

In this section, some initial results available at the assembly level are shown. Figure 16 and Figure 17 show the deformed geometry with a contour plot of residual stresses for an assembly of a flat sheet and a straight, 1.2mm thick, 35mm deep DP590 hat section generated from the NUMISHEET tooling [22]. Figure 16 exhibits directional deformations available along a single path in the same assembly, which becomes an exported result for additional processing into the assembly twist results.

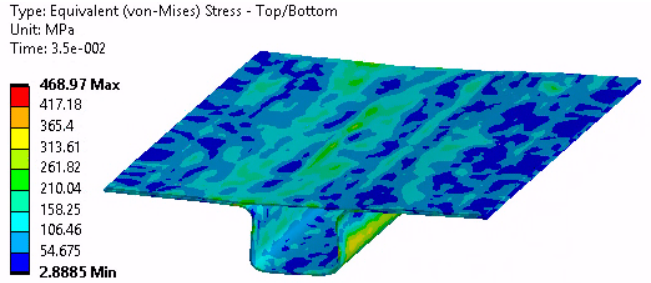

FIGURE 16: EXAMPLE OF DEFORMED GEOMETRY AND RESIDUAL STRESSES IN AN ASSEMBLY

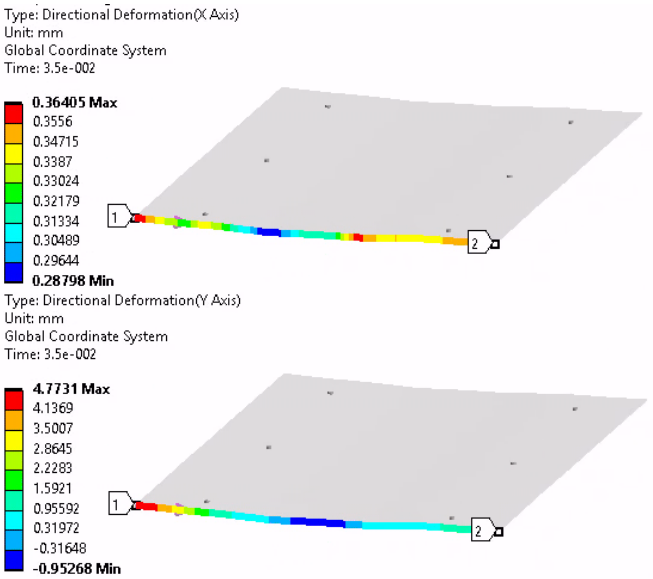

FIGURE 17: EXAMPLES OF DIRECTIONAL DEFORMATIONS ALONG A SINGLE PATH IN A JOINED ASSEMBLY

Table 5: Examples of Calculated Twist Angle Parameters from Assembled Components

Assy type	Twist angle, deg
S-H	0.0925
H-F	0.0847

Table 6: Zone Radii for Component Edges in Two Assemblies

Assy type	Location	Zone radius, mm
S-H	L,T	0.173
S-H	R,T	0.176
S-H	L,B	0.201
S-H	R,B	0.090
H-F	L,T	0.391
H-F	R,T	0.191
H-F	L,B	0.371
H-F	R,B	0.239

At this time the parameters for assessing assemblies are the angle of twist between the front and back profiles, and the radii of cylindrical minimum zones that just capture the sprungback

nodes along longitudinal edges (left or right edges of Figs. 11 and 12). Two assemblies provide data for the results:

Each twist angle is the angle between two lines. The first is the line formed from the two points at the ends of the flanges (corner points) in the front profile, and the second line is formed similarly from the two corner points of the back profile. Since there are nodes in both the upper and lower component of the assembly, the coordinates of each corner point is obtained as the average of values from the two components. Examples of these twist results are shown in Table 5 for one sheet/half-depth assembly (S-H, Figure 12) and one half-depth/full-depth assembly (H-F, Figure 11)

Cylindrical zone radii along the edges of the two assemblies are computed for each component separately to avoid inflating the results by material thicknesses. Therefore, in Table 6 there are eight results (left or right edges, assembly type, and top (T) or bottom (B) component). The method for computing the zones is described in [24].

4.3 Limitations

There are some limitations to consider with respect to the dataset generated using this workflow and its applications in training of ANNs. For instance, the component shapes which have been generated already are fairly simple – much less complex than those used in real assemblies such as automotive bodies. As such, any algorithm trained using this dataset would be limited to drawing conclusions only regarding the simple shapes of this dataset. However, the logic of this workflow could be extended to complex shapes in the future, which would eliminate this limitation. Further, the springback parameters could be made more meaningful and elaborate, especially for assemblies.

Additionally, the accuracy of the results in this dataset is limited by specific simulation settings. Referring back to the modifications made when transitioning from the validated forming simulation, the springback exhibited by formed components after the modifications was shown to be lower than expected. As such, any algorithm trained based on this dataset would only be able to reliably predict relative springback differences between components or relative twist differences between assemblies, as opposed to the absolute values of each. To address this, the validated forming simulation could be used to generate another dataset using this same workflow procedure, requiring additional computing time and power.

Another key limitation to consider for this workflow is the fact that the spot weld model does not consider any thermal effects from the heat affected zone, which has shown to be significant in actual welded flexible assemblies. To include this phenomenon in the workflow would require additional simulations and models which fall outside the scope of this work.

5. CONCLUSIONS

In conclusion, this work has produced an operational simulation workflow and post-processing scheme for generating a curated dataset of results significant for flexible assembly engineered products. The forming simulation was shown to utilize a validated process, the intermediate solutions from each simulation stage were properly transferred to downstream stages, and FE results were extracted and processed into geometric parameters for component springback and for assembly deformations (twist and edge deviations). All of this allows for the curation of this data into a multi-dimensional matrix relating process inputs to key result outputs which, in turn, can be applied to train future ANNs to predict the same results without the need for simulation.

6. FUTURE WORK

With the work and results described, this paper is a progress report. Additional work is underway and will be described in the future. This includes further automating the workflow, which would allow for generation of an even larger dataset and, therefore, better training of ANN algorithms. Additionally, this would allow for further variations to the components and assemblies in the dataset. For instance, including additional materials, thicknesses, and component shapes. Moreover, additional output results such as a residual stress metric and twist in other directions are being considered for addition to the workflow. Finally, a future task of this work would include application of the dataset generated with this workflow toward optimization of process/tooling design or training of an ANN to predict results based on inputs alone, without the need for the finite element simulations performed here.

ACKNOWLEDGEMENTS

The authors are grateful for funding provided to this project by National Science Foundation Award #2029905.

REFERENCES

[1] M. Rajasekaran, V. Hari Ram, and M. Subramanian, “A new minimal part breakup BIW design approach and optimized material map strength assessment,” *J. Teknol.*, vol. 78, no. 7, Jun. 2016.

[2] E. Mclaughlin, T. Gupta, A. Fallaharezadoor, and T. Altan, “Reducing springback in hat-shape bending with variable BHF using servo-hydraulic cushion,” *Stamp. J.*, 2018.

[3] A. Makinouchi, E. Nakamchi, E. Onate, and R. Wagoner, “NUMISHEET ’93,” 1993.

[4] J. Lee, G. Kinzel, and R. Wagoner, “NUMISHEET ’96,” 1996.

[5] J. Gelin and P. Picart, “NUMISHEET ’99,” 1999.

[6] K. P. Li, W. P. Carden, and R. H. Wagoner, “Simulation of springback,” *Int. J. Mech. Sci.*, vol. 44, no. 1, pp. 103–122, 2002.

[7] P. Wollstadt, M. Bujny, S. Ramnath, J. J. Shah, D. Detwiler, and S. Menzel, “CarHoods10k: An Industry-

grade Data Set for Representation Learning and Design Optimization in Engineering Applications," *IEEE Trans. Evol. Comput.*, pp. 1–1, 2022.

[8] S. Ramnath, J. J. Shah, P. Wollstadt, M. Bujny, S. Menzel, and D. Detwiler, "OSU-Honda automobile hood dataset (CarHoods10k)," *Dryad Dataset*, 2022. doi:10.5061/dryad.2fqz612pt.

[9] S. Ramnath *et al.*, "Automatically Generating 60,000 CAD Variants for Big Data Applications," in *International Design Engineering Technical Conferences and Computers and Information in Engineering Conference*, 2019.

[10] S. Ramnath, P. Haghighi, J. Ma, J. J. Shah, and D. Detwiler, "Design Science meets Data Science: Curating Large Design Datasets for Engineered Artifacts," in *International Design Engineering Technical Conferences and Computers and Information in Engineering Conference*, 2020.

[11] S. C. Liu, S. J. Hu, and T. C. Woo, "Tolerance analysis for sheet metal assemblies," *J. Mech. Des. Trans. ASME*, vol. 118, no. 1, pp. 62–67, 1996.

[12] J. A. Camelio and S. J. Hu, "Compliant assembly variation analysis using components geometric covariance," *ASME Int. Mech. Eng. Congr. Expo. Proc.*, pp. 431–437, 2002.

[13] K. G. Merkley, K. W. Chase, and E. Perry, "An Introduction to Tolerance Analysis of Flexible Assemblies," 1996.

[14] B. F. Bihlmaier, "Tolerance analysis of flexible assemblies using finite element and spectral analysis, MSc Thesis," Brigham Young University, 1999.

[15] A. J. Mortensen, "An Integrated Methodology for Statistical Tolerance Analysis of Flexible Assemblies," Brigham Young University, 2002.

[16] ASME Y14.5, "Dimensioning and Tolerancing," *NY Am. Soceity Mech. Eng.*, p. 704, 2009.

[17] R. Söderberg, L. Lindkvist, and S. Dahlström, "Computer-aided robustness analysis for compliant assemblies," *J. Eng. Des.*, vol. 17, no. 5, pp. 411–428, Oct. 2006.

[18] A. Forslund, S. Lorin, L. Lindkvist, K. Wärmefjord, and R. Söderberg, "Minimizing Weld Variation Effects Using Permutation Genetic Algorithms and Virtual Locator Trimming," in *Volume 2: Advanced Manufacturing*, 2017.

[19] D. J. Ceglarek and J. Shi, "Tolerance analysis for sheet metal assembly using a beam-based model," in *American Society of Mechanical Engineers, Design Engineering Division (Publication) DE*, 1997, vol. 94, pp. 153–159.

[20] S. Moos and E. Vezzetti, "Compliant assembly tolerance analysis: guidelines to formalize the resistance spot welding plasticity effects," *Int. J. Adv. Manuf. Technol.*, vol. 61, no. 5–8, pp. 503–518, Jul. 2012.

[21] A. Hashemian and B. M. Imani, "A new quality appearance evaluation technique for automotive bodies including effect of flexible parts tolerances," *Mech. Based Des. Struct. Mach.*, vol. 46, no. 2, pp. 157–167, Mar. 2018.

[22] J. Y. Lee, M.-G. Lee, and F. Barlat, "Evaluation of Constitutive Models for Springback Prediction in U-draw/bending of DP and TRIP Steel Sheets," in *AIP Conference Proceedings*, 2011, pp. 571–578.

[23] Y. He, J. K. Davidson, N. J. Kalish, and J. J. Shah, "Tolerance-Maps for Line-Profiles Formed by Intersecting Kinematically Transformed Primitive Tolerance-Map Elements," *J. Comput. Inf. Sci. Eng.*, vol. 16, no. 2, Jun. 2016.

[24] P. Mohan, P. Haghighi, J. J. Shah, and J. K. Davidson, "Development of a library of feature fitting algorithms for CMMs," *Int. J. Precis. Eng. Manuf.*, vol. 16, no. 10, pp. 2101–2113, Sep. 2015.